The ISME Journal (2021) 15:109–123
https://doi.org/10.1038/s41396-020-00764-2

ARTICLE

To hunt or to rest: prey depletion induces a novel starvation survival strategy in bacterial predators

Rajesh Sathyamoorthy[1] · Yuval Kushmaro[1] · Or Rotem[1,4] · Ofra Matan[1] · Daniel E. Kadouri[2] · Amit Huppert[3] · Edouard Jurkevitch[1]

Received: 16 May 2020 / Revised: 12 August 2020 / Accepted: 25 August 2020 / Published online: 3 September 2020

Abstract

The small size of bacterial cells necessitates rapid adaption to sudden environmental changes. In *Bdellovibrio bacteriovorus*, an obligate predator of bacteria common in oligotrophic environments, the non-replicative, highly motile attack phase (AP) cell must invade a prey to ensure replication. AP cells swim fast and respire at high rates, rapidly consuming their own contents. How the predator survives in the absence of prey is unknown. We show that starvation for prey significantly alters swimming patterns and causes exponential decay in prey-searching cells over hours, until population-wide swim-arrest. Swim-arrest is accompanied by changes in energy metabolism, enabling rapid swim-reactivation upon introduction of prey or nutrients, and a sweeping change in gene expression and gene regulation that largely differs from those of the paradigmatic stationary phase. Swim-arrest is costly as it imposes a fitness penalty in the form of delayed growth. We track the control of the swim arrest-reactivation process to cyclic-di-GMP (CdG) effectors, including two motility brakes. CRISPRi transcriptional inactivation, and in situ localization of the brakes to the cell pole, demonstrated their essential role for effective survival under prey-induced starvation. Thus, obligate predators evolved a unique CdG-controlled survival strategy, enabling them to sustain their uncommon lifestyle under fluctuating prey supply.

Introduction

Natural habitats, like soil and aquatic environments, are often oligotrophic [1, 2]. Accordingly, bacteria have evolved diverse strategies to adapt to changing levels of nutrient availability, including starvation. For example, nutrient depletion in growing populations rapidly brings about a shift to the stationary phase, characterized by different morphological, molecular, and physiological adaptations that lead to growth arrest [3–5]. Changes in environmental conditions can bring about the reactivation of growth-arrested cells, which also can take many routes [6–8].

The obligate predatory bacteria *Bdellovibrio* and like organisms (BALOs) present a peculiar case as they require gram-negative prey to replicate and complete their life cycle. During the attack phase (AP), a free-living, highly motile cell essentially blocked in a non-replicative state with limited cellular growth, searches for prey. Upon encounter, the predator attaches to the prey, and in most BALOs, like *Bdellovibrio bacteriovorus*, it penetrates the prey's periplasm, forming a bdelloplast. Within the bdelloplast, it grows as a filamentous, coenocytic cell, which upon depletion of the prey cell content, synchronously splits to form progeny AP cells that release themselves to the environment [9–11]. Rapid swimming of AP cell is effected by a polar flagellum [12, 13] and depends upon high endogenous respiration rates, and high energy expenditure [14]. In the absence of exogenous respirable material, rapid cell carbon depletion ensues within a few hours, but

Supplementary information The online version of this article (https://doi.org/10.1038/s41396-020-00764-2) contains supplementary material, which is available to authorized users.

✉ Edouard Jurkevitch
edouard.jurkevitch@mail.huji.ac.il

[1] Department of Plant Pathology and Microbiology, Faculty of Agriculture, Food and Environment, The Hebrew University of Jerusalem, 76100 Rehovot, Israel

[2] Department of Oral Biology, Rutgers School of Dental Medicine, Newark, NJ, USA

[3] Bio-statistical Unit, The Gertner Institute for Epidemiology and Health Policy Research, Chaim Sheba Medical Center, Tel Hashomer, Israel

[4] Present address: Seed-x., Magshimim, Israel

survival is little compromised, as measured by the ability of the population to prey [15]. Although differences occur between strains, survival can be drastically reduced within 10 h of prey depletion [15].

BALOs are ubiquitous in oligotrophic environments like soils, seas, lakes, and elsewhere [11, 16]. It has been calculated that a minimal concentration of 7×10^5 prey cell mL^{-1} is necessary to prevent predator eradication [17, 18]. As BALO strains sharing the same environment may differ in prey range and show differential predatory abilities between prey strains [19–21], finding sufficient prey may be challenging. Although total BALO's are quite abundant [22, 23], individual strains may survive at a very low concentration while rapidly responding and growing upon increasing prey availability [19, 24]. Understanding how BALOs survive prey depletion is not only important for understanding their impact on bacterial communities, it is necessary for a judicious application of their predatory abilities. Indeed, treatments with BALOs are drawing increasing attention in medicine, aquaculture, and agriculture as a strategy against antibiotic-resistant bacteria, and to provide environmentally friendly solutions, respectively, for the control of pathogens [25–27].

Here, we find that as AP populations mature under prey depletion-induced starvation after exiting the bdelloplast, they gradually stop swimming over hours, altering swimming patterns, and energy metabolism until total arrest. However, although motility is an absolute requirement for predation, cell survival is minimally altered [12]. We solve this conundrum by showing that the arrested population is reactivated within minutes, resuming swimming after the introduction of prey, yet incurring a fitness cost. We trace the cause of this behavior to specific regulators, including effectors controlled by the secondary signal cyclic-di-GMP (CdG), and demonstrate, using CRISPR interference that CdG-motility effectors are essential for survival under prey depletion.

Results

Attack phase cells vary in size

When looking at overnight predatory co-cultures of *B. bacteriovorus* with prey by light microscopy, we routinely found differently sized AP cells and observed, as reported by Fenton et al. [9] that cells freshly emerged from bdelloplasts (thereafter AP1 cells) were shorter than cells incubated for a few hours. Using flow cytometry, AP1, and older AP cells were readily distinguished (Fig. S1C, D). We further characterized these subpopulations for predation, motility, energy production, changes in transcriptional profile, viability, and survival.

Swimming patterns are altered with cell maturation

In the absence of prey, synchronous *B. bacteriovorus* HD100 (a soil bacterium and the species' type strain) AP cells exhibited a transient increase in swimming speed 2.5 and 5.5 h after their release from the bdelloplast. However, the number of swimming tracks (which represents swimming cells) significantly decreased from 2.5 h onwards (ANOVA with Tukey test, $P < 0.05$). After 8 h of starvation, a large majority of cells did not swim (Fig. 1a–c). As a comparison, *B. bacteriovorus* 109J, also isolated from soil but exhibiting different phenotypic characteristics [28], was tested. Strain 109J's swimming speed and the number of trajectories observed gradually decreased from AP1, starting at 1.5 h, until almost all cells stalled by 4.5 h (Fig. 1d–f). To clarify, we define AP2 populations as those exhibiting a significant decrease in swimming tracks in comparison to AP1 populations; they become arrested AP2 (aAP2) populations when >90% of the cells do not swim. Thus, under our experimental conditions, AP2 lasts from about 2.5 to 8 h, and from 1.5 to 4.5 h, in HD100 and 109J, respectively (Fig. 1c, f).

During this hours long transition, the swimming populations decayed exponentially in time (Fig. S2). Our previous study showed that AP cells from fresh nonsynchronous cultures of *B. bacteriovorus* produce three types of tracks viz., rotatory, curvilinear, and linear tracks [28]. Here, the trajectories of swimming synchronous AP1 cells of both predator strains were mostly rotatory or curvilinear (Fig. 1b, e). Strikingly, the distribution shifted toward linear tracks starting at 2.5 and 1.5 h in strains HD100 and 109J, respectively, i.e., concomitant with a decrease in the number of tracks (Kolmogorov–Smirnov test, $P < 0.001$) (Fig. 1c, f).

Reactivation of aAP2 cells

After 10 h, *B. bacteriovorus* HD100 aAP2 cells were almost uniformly arrested (Fig. 1a, b). However, exposure of this population to *Escherichia coli* (*E. coli*) ML35 at a ratio of 100:1 (predator:prey) elicited a rapid response as, within 60 s, a significant increase in swimming speed and swimming tracks was observed (Fig. 1a, b), defining the reactivated rAP2 population. Qualitatively, the reactivation response of aAP2 cells to *E. coli* cells was similar in both strains HD100 and 109J but exhibited different swimming patterns (Fig. 1e, f). Linear swimming of HD100 cells significantly decreased in time after reactivation (Kolmogorov–Smirnov test, $P < 0.001$) while 109J swimming patterns were hardly affected (Fig. 1b, e).

Effect of starvation on predation dynamics

The effect of starvation on predation dynamics was measured in real time by following fluorescence in predators

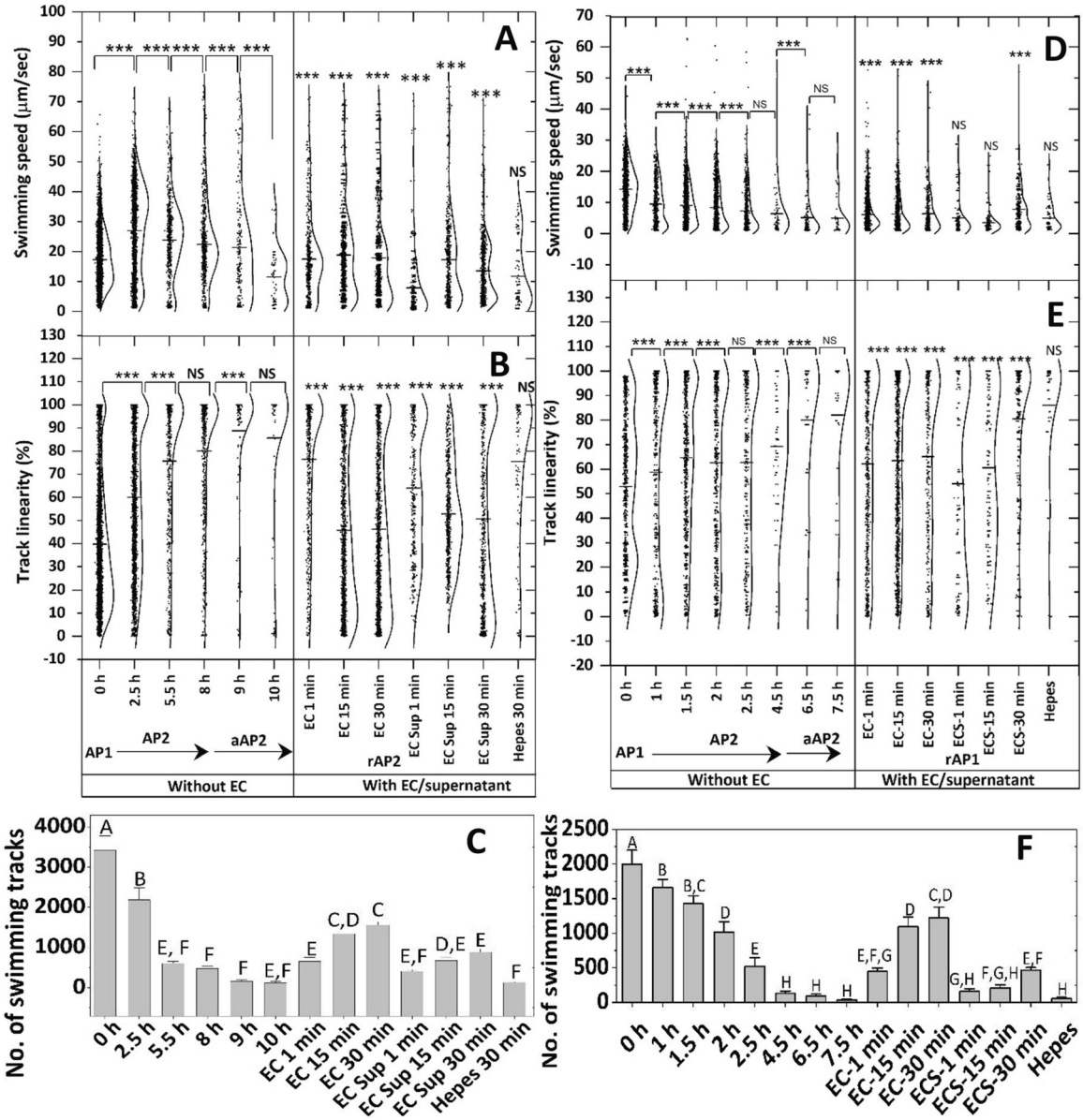

Fig. 1 Changes in motility of *B. bacteriovorus* with time under starvation, and after adding prey. Strains HD100 (**a**–**c**) and 109I (**d**–**f**). **a**, **d** Swimming speed; **b**, **e** Track linearity, i.e., the proportion of linear, curvilinear, and rotating tracks; **c**, **f** Number of swimming tracks. For details on swimming speed and track measurements see Supplementary Materials and Methods. The distribution curves were plotted by Gaussian Kernel smoothing of >3000 individual swimming tracks. Differences between distributions were tested using the Kolmogorov–Smirnov test. Levels connected by *** stand for significant differences at $P < 0.005$ and NS denotes differences that are not significant ($P > 0.05$). The aAP2 was compared to rAP2. Bars in **c**, **f** not connected by the same letter are significantly different (Tukey's test at a 0.05% significance level). The horizontal line in **a**, **b**, **d**, and **e** represents mean. For definitions of AP1, AP2, aAP2, and rAP2 see text; EC *Escherichia coli*, ECS *E. coli* supernatant, AmHEPES control.

expressing the *tdTomato* gene. Both *B. bacteriovorus* HD100-TdTomato and *B. bacteriovorus* 109J-TdTomato cultures exhibited similar dynamics, reaching maximal population sizes about 10 and 6 h earlier, respectively, when inoculated with AP1 cells as compared with aAP2 cells (starting predator: prey ratio, 1:1000, Student *t* test, $p < 0.001$) (Fig. S3A, B). This suggests that swim-arrested cells are at a competitive disadvantage compared to swimming cells.

aAP2 cells are reactivated by bacteria, growth media, and amino acids

Since *E. coli* cells had a pronounced reactivation effect on aAP2 cells, the effects of another prey bacterium, *Klebsiella oxytoca*, as well as, Gram-positive non-prey *Micrococcus* sp., rich nutrient media, and specific amino acids were explored, using strain HD100. In most treatments with prey cells, culture supernatants or complex media, exposure of

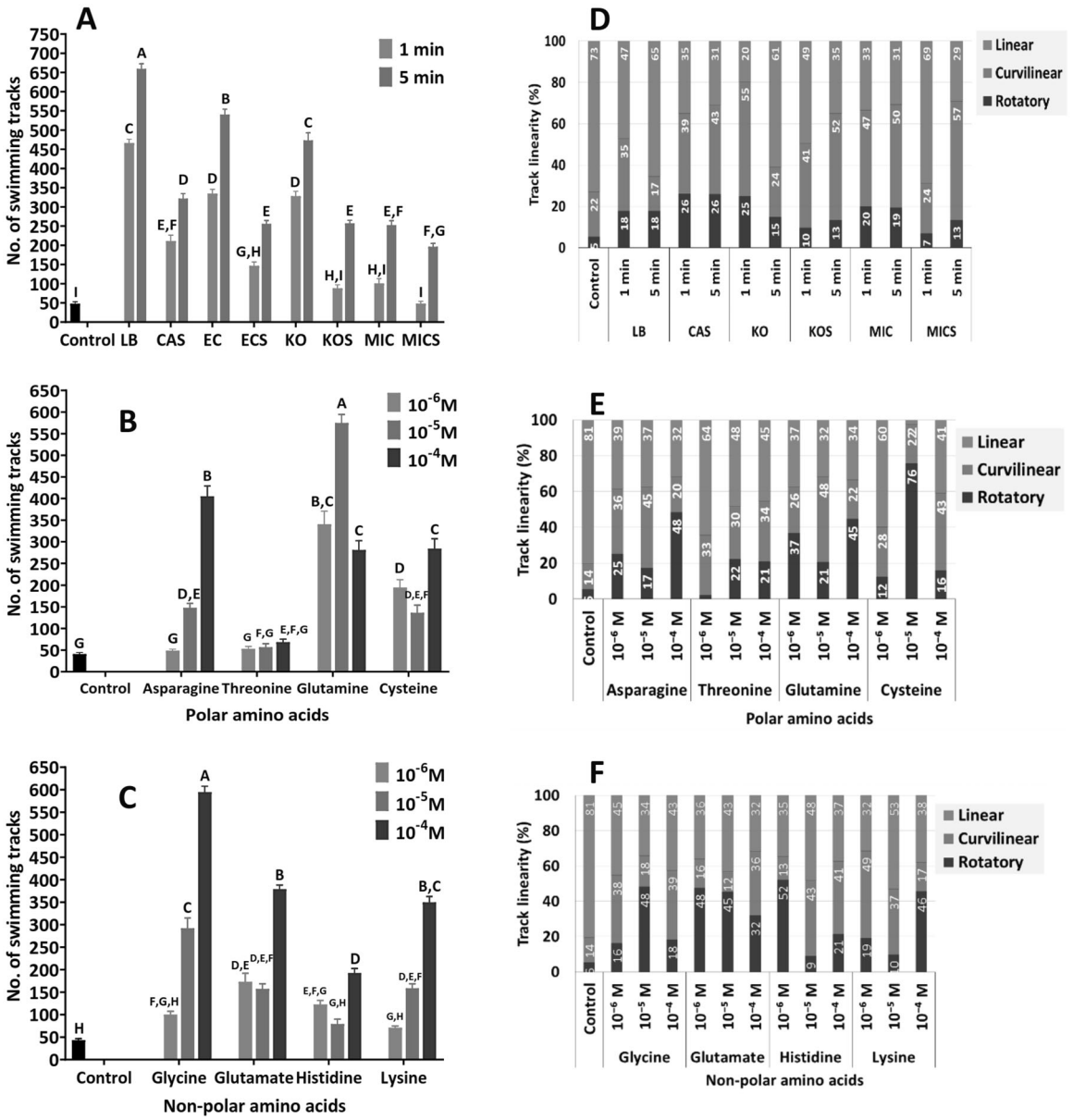

Fig. 2 Changes in the motility of *B. bacteriovorus* HD100 aAP2 cells exposed to various elicitors. Changes in the number of swimming tracks (**a**–**c**), upon exposure to: **a** Prey, non-prey, and rich media; **b** Polar amino acids; **c** Nonpolar amino acids; in the proportion of linear, curvilinear and rotating tracks (**d**–**f**) upon exposure to: **d** Prey, non-prey, culture supernatants, and rich media; **e** Polar amino acids; **f** Nonpolar amino acids. For details on swimming speed and track measurements see Supplementary Materials and Methods. Bars show mean values and standard error of the mean. Levels not connected by the same letter are significantly different by Tukey's test at a 0.05% significance level. Control, the fraction of swimming cells within the aAP2 population (<5%) with amHEPES added; EC *Escherichia coli*, ECS *E. coli* concentrated (×10) culture supernatant, KO *Klebsiella oxytoca,* KOS, *K. oxytoca* concentrated (×10) culture supernatant, CAS casamino acids, MIC *Micrococcus* sp., MICS *Micrococcus* sp. concentrated (×10) culture supernatant, LB Lysogeny broth.

aAP2 cells led to a significant reactivation of swimming within 60 s, as measured by counting swimming tracks. All treatments had a strong effect within 5 min (Fig. 2a). *E. coli*, *Klebsiella* prey cells, and their concentrated culture supernatants reactivated aAP2 to different extents but significantly more than *Micrococcus* cells, that reached 45.5% of the level obtained when using *E. coli* (Fig. 2a). In most cases, the proportion of linear tracks in the rAP2 populations decreased concomitantly with an increase in curvilinear and rotatory tracks. These were significantly different than the tracks observed in amHEPES-exposed control cells (81% linear, Fig. 2d). Control cells are the cells within the aAP2 population that remain swimming after 10 h of prey starvation (Figs. 1c, 2; <5%).

The reactivation potential of amino acids on aAP2 cells, generally positively correlated with increased concentrations.

The polar amino acids glutamine and asparagine and the nonpolar amino acids, glycine, and glutamate largely increased reactivation compared to control aAP2 cells. The resulting swimming patterns differed between each amino acid and its concentrations, but all greatly differed from the linear pattern of the control tracks (Fig. 2b–f). The other tested amino acids were weakly effective, except threonine, which did not have an effect on the number aAP2 tracks (Fig. 2b, e).

Changes in ATP, membrane potential, and cell viability

ATP levels largely dropped at the onset of AP2, increasing in aAP2 populations (ANOVA with Tukey test, $P > 0.05$) (Fig. S4A). Upon *E. coli*-induced reactivation, ATP increased by 2.5 times within 5 min; yet no increase was observed in cells reactivated with LB despite the increase in swimming tracks (Figs. 2a, S4A). Differences were also measured in membrane potential, being higher in AP2 and rAP2 than in AP1, while few differences were observed between the reactivation treatments (Fig. S4B). Viability, as determined by the live/dead stain, was not affected, even after 8 h of starvation (Fig. S4B, C). Thus swim-arrest does not result from cell energy depletion.

Gene expression is significantly altered between AP1 and aAP2 populations

To examine whether AP1 and aAP2 populations differ in gene expression, we performed an RNA sequencing experiment to compare the transcriptome profiles of both. A summary of the differences is depicted as a circular map (Fig. 3a). As illustrated in Figs. 3b, S5A, principal component analysis and a heat map, respectively, show that AP1 populations considerably differ from aAP2 populations. Of the 3586 genes in *B. bacteriovorus* HD100 genome, 935 genes were differentially expressed (differentially expressed genes-DEGs). Five hundred and forty genes were upregulated, and 395 were downregulated in aAP2 populations as compared to AP1 populations (Fig. 3c). A COG enrichment analysis of differentially aAP2 expressed genes in comparison with AP1 revealed that aAP2 genes involved in posttranslational modification, protein turnover, and chaperones (8%); transcription (7%); carbohydrate transport and metabolism (6.2%); translation and ribosomal structure and biogenesis (6.2%) and signal transduction mechanisms (4.4%) were all upregulated (Fig. S5B).

The expression of the cyclic-di-GMP (CdG) gene network is altered during swim arrest and reactivation

The *B. bacteriovorus* HD100 genome encodes 114 genes involved in CdG signaling (Fig. S6). Of these, 20 (18%), and six (5%) genes were upregulated and downregulated in aAP2, respectively, compared to AP1 (Fig. 4a, Table S1). More specifically, *bd1434*, (*dgcC)*, a diguanylate cyclase that strongly affects the predator's life cycle [29], was upregulated in aAP2 and went down 27-fold in rAP2, as was the expression of *merRNA*, a putative CdG standalone riboswitch [30] (Fig. 4b). In contrast, the expression of the phosphodiesterase genes, *bd2325* and *bd2421* was significantly upregulated upon cell reactivation (Fig. 4b). Out of 18 PilZ domain-containing genes (PilZ is canonical CdG-binding domain, [31]), 10 were differentially expressed (Fig. 4c). As these genes encode for hypothetical proteins, putative functions were predicted by sequence analysis using the SWISS model and Phyre2. Among these, Bd1007 and Bd0760, whose encoding genes were upregulated 4 and 8 fold, respectively, in aAP2 cells, were found to be structurally similar to a protein in *P. putida* that shares low sequence homology to the flagellar-brake YcgR [32, 33] (Fig. S7). When individually overexpressed in *E. coli* K12, both genes affected swarming and swimming motility similarly to that observed with the *E. coli* flagellar-brake protein YcgR (ANOVA with Tukey test, $P < 0.001$) (Fig. S8). Taken together, the data strongly suggested that these proteins are functional analogs of the molecular brake YcgR.

Mutations of CdG effectors alter swim-reactivation dynamics

Since the levels of diguanylate cyclase, *dgcC* (*bd1434*) and *merRNA* were found to be differently expressed between aAP2 and rAP2, their effect on swim-reactivation were assessed using a two-chambered slide with a narrow transition path to measure the time taken by starved non-swimming aAP2 cells to reach a chamber containing *E. coli*. Reactivation of *ΔmerRNA* and *ΔdgcC* aAP2 cells was significantly slower than in the wild-type, lasting on average about 15 and 20 min, compared to about 1.8 min, respectively (Fig. 4d). The *ΔmerRNA* strain complemented with a chromosomal insertion of the wild-type *merRNA* was restored to the original phenotype (Fig. 4d). These results, along with the identification of PilZ, domains in Bd0760, and Bd1007 strongly support a central role for CdG signaling in swim reactivation.

Bd0760 and Bd1007 are localized at the polar end

In order to pinpoint where the flagellar-brake proteins may act, in-frame *gfp-bd0760* and *gfp-bd1007* fusions were separately tested. Both fusion proteins displayed punctuated fluorescence at the polar end of *B. bacteriovorus* HD100 aAP2 and a faint, non-localized signal in AP1 (Fig. 4e–h).

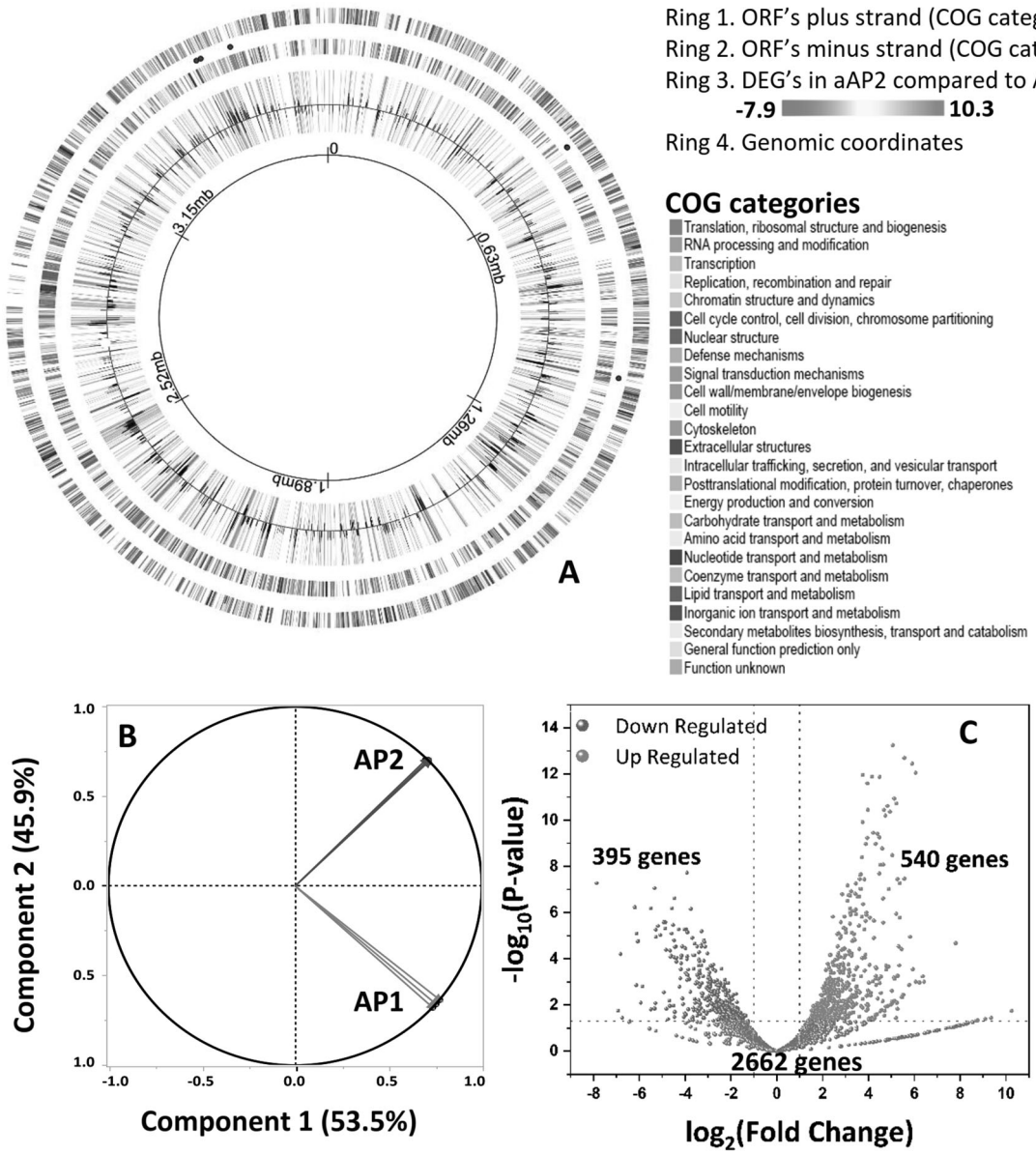

Fig. 3 Comparative transcriptomic analysis of *B. bacteriovorus* HD100 motility-arrested attack phase cells (aAP2) and fresh attack phase cells (AP1). a Circular maps represent the *B. bacteriovorus* HD100's transcriptome. Rings, from the outside to the inside: rings 1 and 2 denote open reading frames (ORF's) on the plus and minus strand (color coded by Cluster of Orthologous Group (COG) categories); ring 3 denotes transcripts differentially expressed in aAP2 compared to AP1. **b** Principal component analysis plot from gene expression values comparing AP1 and aAP2. **c** Volcano plot of differentially expressed genes (DEG's) of aAP2 compared to AP1 (False discovery rate (FDR) adjusted p value < 0.05; log2 fold change > 2). Spots in the left and right quadrants indicate significantly down and upregulated genes, respectively. Spots in the gray area represent genes that are neither over nor under expressed. NS—not significant. This plot was generated using a circular visualization of microbial genomes (CiVi; http://civi.cmbi.ru.nl/).

Bd0760 and Bd1007 regulate motility and survival

Gene silencing was used to measure the effect of Bd0760 and Bd1007 on the swim-arrest-reactivation process. To this end, a CRISPRi (interference) system was constructed in pRdcas9 carrying a kanamycin resistance cassette (Fig. S9A, B). Interference was tested using the red fluorescent protein *tdTomato* under a PnptII promoter in pMQ414 carrying gentamicin resistance, conjugated in both *B. bacteriovorus* HD100 and 109J carrying pRdcas9 sgRNA targeting *tdTomato* (Fig. S9C–E). Both plasmids were stably maintained. Predation of an *E. coli* prey tracked by real-time fluorescence analysis showed a 4.7-fold decrease in tdTomato fluorescence in the CRISPRi strains targeting *tdTomato* compared to the pRdcas9 empty sgRNA (Emp-sgRNA) (Fig. S9F, G),

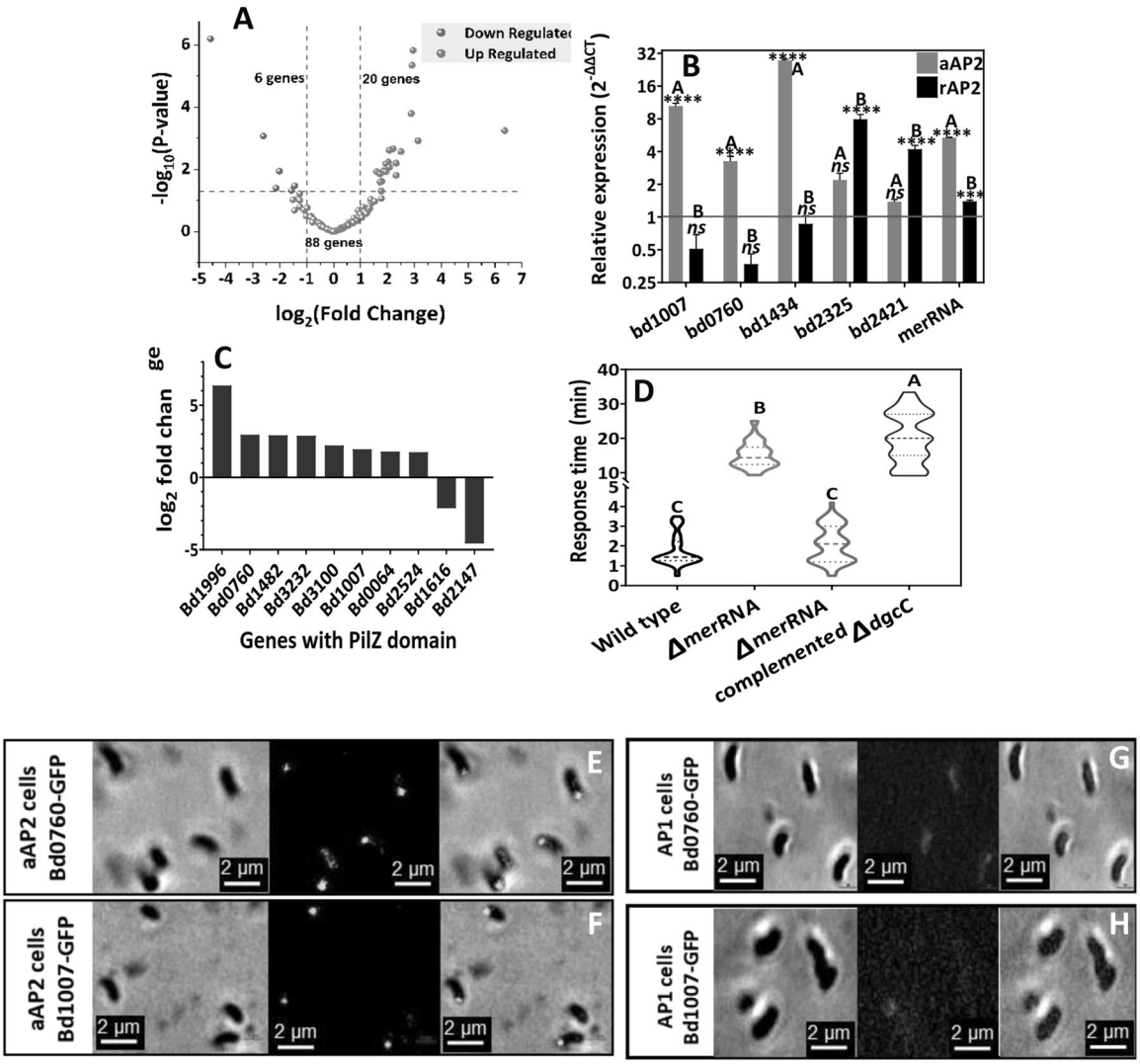

Fig. 4 Changes in expression levels of cyclic-di-GMP (CdG) signaling-related genes in *B. bacteriovorus* HD100. a Volcano plot depicting CdG differentially expressed genes (DEG's) of motility-arrested attack phase cells (aAP2) compared to fresh attack phase cells (AP1) (False discovery rate (FDR) adjusted p value < 0.05; log2 fold change > 2). Spots in the left and right quadrants indicate significantly down and upregulated genes, respectively. Spots in the gray area represent genes which are neither over nor under expressed. **b** Quantitative PCR validation of *bd1007, bd0760, bd1434, bd2325,* and *bd2421* genes and of *merRNA* in AP1, aAP2, and rAP2 exposed to *E. coli* (EC) for 30 min. AP1 expression is 1 (horizontal line). The expression of the other genes is relative to it. **c** Differentially expressed genes with a CdG-binding pilZ domain. **d** Response time for the wild type, *ΔmerRNA* and *ΔdgcC* (diguanylate cyclase, *Δbd1434*) mutant strains in aAP2 to the addition of *E. coli* to a microfluidic device. **e**–**h** aAP2 Bd0760-GFP (**e**), aAP2 Bd1007-GFP (**f**), aAP2 Bd0760-GFP (**g**), and aAP2 Bd1007-GFP (**h**) localization (scale bar, 2 μm). The genes were expressed under their native promoter. *bd1434*, diguanylate cyclase (*dgcC*); *bd2325* and *bd2421*, phosphodiesterases; *bd0760* and *bd1007, ycgR*-like flagellar brakes, *merRNA*, noncoding putative CdG riboswitch I. In **b**, bars not connected by the same letter are significantly different by Tukey's test at 0.05% significance level. In qPCR data, AP1 was compared to aAP2 and rAP2 using paired sample Student t test. **** and *** denotes significant differences at $p <$ 0.0001 and $p < 0.01$ level. ns denotes non-significance. For any gene, differences between aAP2 and rAP2 are denoted by different letters.

with no significant difference in final population level (Fig. S10A, B).

Thereafter, *bd0760* and *bd1007* were individually silenced using the CRISPRi system, yielding strains Sil-*bd0760* and Sil-*bd1007*. The number of tracks in synchronous cultures significantly decreased from AP1 to AP2 to aAP2 in Sil-*bd0760*, Sil-*bd1007*, and in control strain Emp-sgRNA (Fig. 5a–c). Sil-*bd0760* and Sil-*bd1007* reached aAP2 18 and 22 h after progeny release, respectively, as compared to 10 h for Emp-sgRNA (Fig. 5a, d, g). Strikingly, prey-induced reactivation of aAP2 Sil-*bd0760* and Sil-*bd1007* was largely reduced, as no significant increase in the number of swimming tracks was detected 1 h after exposure. This was in contrast to resumed swimming in

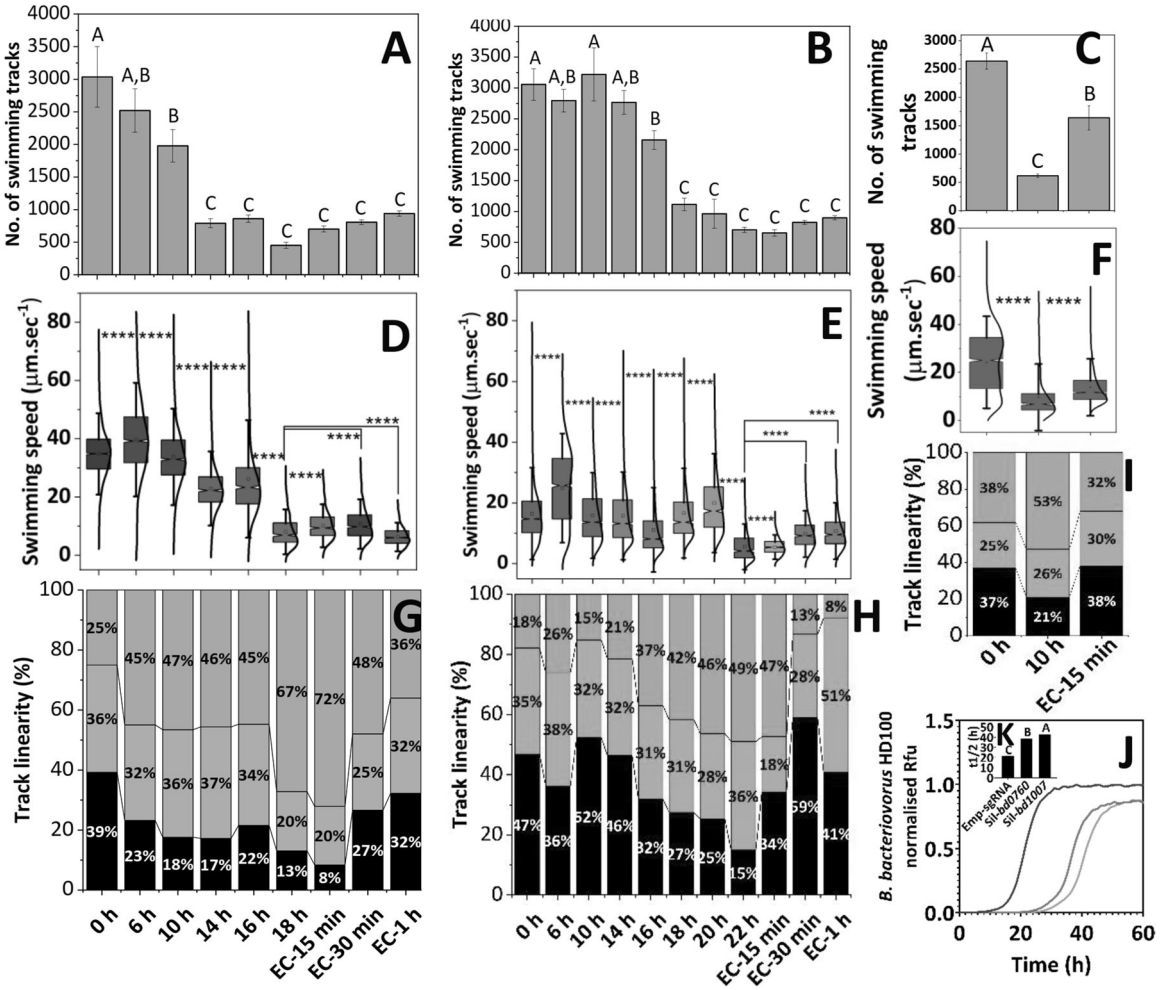

Fig. 5 Changes in motility and predation dynamics in *B. bacteriovorus* HD100 silenced for break proteins expression. Strain silenced in *bd0760* (**a**, **d**, **g**), *bd1007* (**b**, **e**, **h**), or carrying an empty pRdcas9 vector (**c**, **f**, **i**) using CRISPRi-mediated flagellar-brake genes repression. Number of swimming tracks (**a**–**c**); Swimming speed (μm sec^{-1}) (**d**–**f**); Track linearity (**g**–**i**.). **j** Real-time predation dynamics, captured by measuring tdTomato fluorescence expressed in wild-type strain HD100 and in the strains silenced for *bd0760* (red line) or *bd1007* (green line) expression, or carrying an empty pRdcas9 vector. The inset shows predation efficiency as half-life (t1/2, the time in h to reach growth phase midpoint (**k**)). For details on swimming speed and track measurements see Supplementary Materials and Methods. The distribution curves were plotted by Gaussian Kernel smoothing of >3000 individual swimming tracks. Differences between distributions were tested using the Kolmogorov–Smirnov test. Levels connected by **** stand for significant differences at $P < 0.0001$. Bars in **a**–**c**, **j** not connected by the same letter are significantly different by Tukey's test at a 0.05% significance level. EC *E. coli* ML35.

Emp-sgRNA after 15 min (ANOVA with Tukey test, $P < 0.05$) (Fig. 5b, e, h). Although in Sil-*bd0760* and Sil-*bd1007* the number of swimming tracks did not increase after exposure to *E. coli*, their path distribution exhibited a shift similar to Emp-sgRNA (Fig. 5c, f, i). Lastly, predation dynamics of *bd0760*, Sil-*bd1007*, and Emp-sgRNA transformed with pMQ414-*tdTomato* was measured by real-time fluorescence, revealing that the maximal population size reached by *bd0760* and *bd1007* at 17 and 21 h was about 30% lower than that reached by Emp-sgRNA, at the same time point (starting predator:prey ratio, 1:1000; ANOVA with Tukey test $P < 0.05$) (Fig. 5j, k). We concluded that Bd0760 and Bd1007 act as molecular brakes that affect the swim-arrest and reactivation response.

Sigma factors are differentially expressed and affect gene expression in AP1 vs. aAP2

B. bacteriovorus HD100 has seven sigma factors; of these, four were found to be differentially expressed in aAP2 when compared to AP1 (Fig. 6a). The housekeeping sigma factor *bd0242-rpoD* was downregulated in aAP2 along with *rpoH* and *rpoE*, that encode for heat shock and extracytoplasmic stress response functions, respectively. Sigma factor *fliA* (*bd3318*, a major controlling factor of flagellar genes) was found to be upregulated in aAP2 (Fig. 6b). In total, 151 genes are under the control of *fliA* regulation [30]. Of these, 48 genes were upregulated and two genes were downregulated in aAP2 compared to AP1 (Fig. 6c). Among these

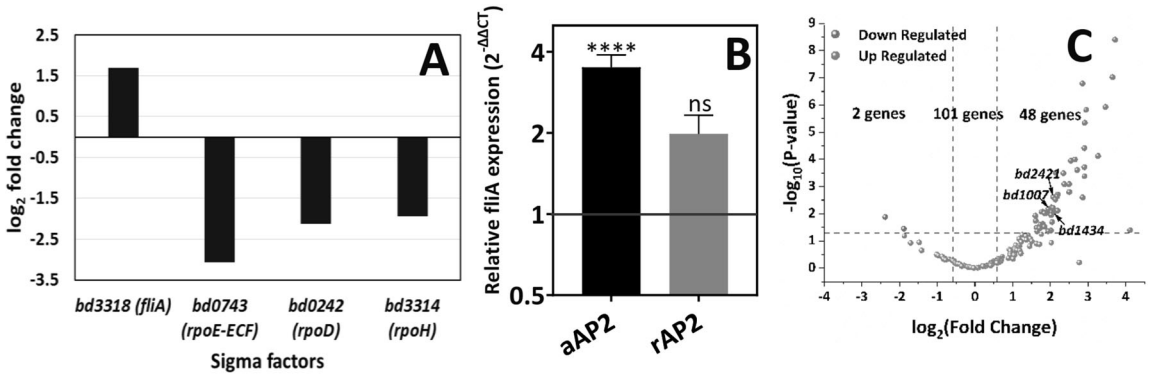

Fig. 6 Transcriptional changes in sigma factors in *B. bacteriovorus* HD100 motility-arrested attack phase cells (aAP2) compared to fresh attack phase cells (AP1). a Differential expression of sigma factors in aAP2 compared to AP1. **b** Quantitative PCR validation of the expression of *bd3318* (*fliA*) in AP1, aAP2, and rAP2 exposed to *E. coli* (EC) for 30 min. AP1 expression is 1 (horizontal line). The expression of the other genes is relative to it. **c** Volcano plot depicting the differential expression of aAP2 genes under the control of the *bd3318*(*fliA*) sigma factor compared to AP1 (False discovery rate (FDR) adjusted p value < 0.05; log2 fold change > 1.5). In QPCR data, AP1 was compared to aAP2 and rAP2 using paired sample Student t test. **** denotes significant differences at $p < 0.0001$ level. ns denotes—non significance.

151 genes, 16 genes were found to take part in CdG signaling, including *bd1007* and *bd0760*, *dgcC*, and *bd2421*.

Differential expression of other genes

All *B. bacteriovorus* stress-related genes (Gene ontology id: GO:0006950) were upregulated by at least twofold in aAP2 compared to AP1 (Table S1). Most of the transcriptional regulators, one-component system-related genes, and response regulators were found to be upregulated in aAP2 compared to AP1 (Table S1). Apart from differential expression in the noncoding *merRNA*, noncoding RNAs ApsRNA3 and APsRNA4 [30] were highly expressed in aAP2. These ncRNAs are located upstream of flagellin genes that are also upregulated in aAP2 suggesting that they may be involved in the regulation of flagellar synthesis.

Discussion

B. bacteriovorus HD100 and 109J are both soil bacteria. Although closely related, they differ in prey range [34], in genomic content [35, 36], in predation rate, and swim differently under various conditions [28]. Yet, the swim arrest-reactivation phenomenon was observed in both, with variations (Figs. 1, S3A, B), suggesting it is a general adaptation of *B. bacteriovorus* to prey deprivation.

Swim-arrest implies a fundamental physiological shift, reflected in the very large number of genes (935/3586, 26%) differentially expressed between AP1 and aAP2 (Figs. 3, S5). The aAP2 gene expression pattern bore limited resemblance to the *E. coli* starvation response: the oxidative stress response catalase (*catA*) (*bd0798*), the DNA protection during starvation protein (*dps*) (*bd2620*) and the 70S ribosome hibernation protein gene *raiA* (ribosome associated factor *Y/yfiA*) were strongly upregulated [37]. However, the stress-related *rpoH* and *rpoE-ECF*, and the housekeeping *rpoD* sigma factors were downregulated in aAP2. At the same time, *fliA*, a sigma28 factor, regulating motility in many Gram-negative bacteria [38, 39], which controls about two-thirds of the AP-specific program in *B. bacteriovorus* [30, 40] was upregulated, driving the expression of 50 proteins (Fig. 6c). This was in sharp contrast to what can be observed in the paradigmatic early stationary phase [41]. Lastly, *rpoS*, the major stationary phase-related sigma factor of many Gram-negative is not present in *B. bacteriovorus* [37, 42], and aAP2 cells did not show size reduction, a hallmark of the stationary phase [43]. Consequently, we suggest that swim-arrest in *Bdellovibrio* defines a rather unique response in the face of prey depletion, and not a mere adaptation of the classical starvation/entry into stationary phase. Such cellular hedging, a behavior recently proposed to maximize survival under environmental versatility [44], may be particularly beneficial for soil microorganisms [45, 46], and *B. bacteriovorus* predators, in particular, because of the rapid spatiotemporal changes in their chemical, physical, and biological environments [47–49] (see below).

In a number of bacteria, a network of diguanylate cyclases and phosphodiesterases modulates CdG cellular concentration [50]. At high levels, and under nutrient starvation, the secondary messenger binds at the PilZ domain of YcgR, a FliA-regulated [38, 39] flagellar molecular brake, which in turn regulates swimming and swarming by binding to elements of the flagellar motor (MotA) [51] and/or FliG and FliM [52], causing the motor to slow down. Here we show that in *B. bacteriovorus*, CdG plays a central role in modulating motility under prey depletion: *dgcC* and *merRNA*, were upregulated during swim-arrest but

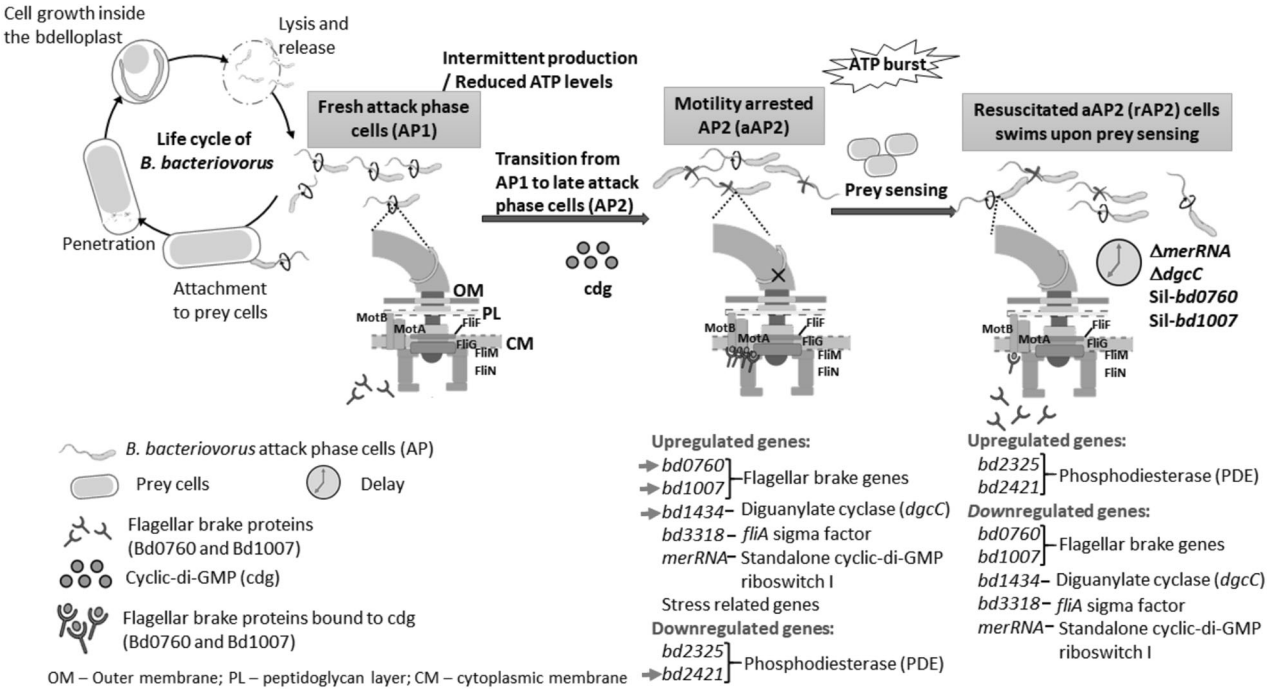

Fig. 7 The life cycle of the periplasmic predator *Bdellovibrio bacteriovorus* (left). Fresh attack phase (AP1) cells emerge from the bdelloplast. Flagellar brakes are lowly expressed and the bacterium swims in mostly rotational/curvilinear paths. In the absence of prey, AP1 cells mature to AP2 that experience decreased ATP production along with an increase in linear swimming, their swimming exponentially decaying over hours until almost all cells are arrested aAP2 cells (center). In aAP2 cells, the Bd0760 and Bd1007 flagellar brakes are highly expressed, as is the cyclic-di-GMP (CdG) synthesizing diguanylate cyclase enzyme DgcC and the putative CdG riboswitch *merRNA*. CdG binds to the brakes' PilZ domain enabling them to interact with the flagellum's motor (here the stator, as an example) and stop its rotation. Upon the addition of prey (right), CdG-breakdown phosphodiesterase enzymes are upregulated, the flagellar brakes are downregulated as are *dgcC*, *merRNA,* and the flagellar regulator *fliA*, bringing about rapidly renewed rotational/curvilinear swimming as ATP production bursts. Mutations in *merRNA* or in *dgcC* strongly delay reactivation. CRISPRi interference of *bd0760* and *bd1007* expression cancels rAP2, significantly slowing down predatory growth and reducing final predator population sizes. FliA-regulated genes are pointed by red arrows.

downregulated upon prey sensing. In contrast, upon prey sensing and reactivation, the expression of the phosphodiesterase genes *bd2325* and *bd2421* increased (Fig. 4). Furthermore, the *ΔdgcC* and *ΔmerRNA* strains exhibited significant delays in swim reactivation (Fig. 4d), and double *dgcC* and *merRNA* mutants could not be obtained in a screen of about 300 plaques (not shown) suggesting they interact in an essential manner. Furthermore, PilZ domain-bearing proteins Bd0760 and Bd1007, which were upregulated in aAP2 functionally complemented the orthologous YcgR in *E. coli* (Fig. S8). Strikingly, transcriptional inactivation using a novel CRISPRi system showed both Bd0760 and Bd1007 were essential to achieve the rapid response observed in reactivation experiments. Remarkably, inactivation strongly affected survival under prey depletion by imposing very long growth delays and reduced population sizes; as in the wild-type strain, it did not hinder the response to prey and the restoration of rotational/curvilinear dominance (Fig. 5). Figure 7 summarizes these findings.

What could be the ecological advantage of such a swim arrest-reactivation mechanism? In soil and aquatic habitats where BALOs dwell, the supply of prey may be fluctuating or unequally distributed in space [53, 54]. Under prey deprivation, the number of swimming cells decayed exponentially over hours, the velocity of AP cells decreased with starvation time concomitantly with an increase in linear swimming (Fig. 1a, b) until swim-arrest. However, in reactivated rAP2 cells, this linearity dissipated with an increase in rotational tracks (Figs. 1b, 2d–f). AP cells can swim extremely fast [12], certainly requiring much energy as bacterial flagellar rotation is proportional to the proton motive force [55]. We observed that both the average membrane potential and velocity transiently increased at the onset of starvation (Figs. 1a, S4) to then decrease. Remarkably, ATP levels decreased within hours, rising somewhat as arrested aAP2 cells accumulated. Gadkari and Stolp [56] showed that in *B. bacteriovorus* 109J, ATP levels oscillate with a downward trend within 2–3 h of starvation, with energy periodically produced in the absence of exogenous substrate. In *Salmonella typhimurium* ATP is required for normal clockwise rotation (Shioi et al. [57]), to bring about directional change. So, increased linear swimming and

reduced swimming speed as observed here, may conserve energy, in line with the increase in smooth swimming controlled by YcgR and modulated by CdG seen under nutrient depletion in *E. coli* [51, 58]. It is noteworthy that increased linear swimming in BALOs was also observed under high viscosities and was concomitant with increased predatory efficiency at low prey concentrations [17], a condition known to be challenging for the predator [17, 59]. Thus, under such stresses, a shift in swimming patterns, by conserving energy, may increase prey search time. *B. bacteriovorus* AP1 cells emerging from a bdelloplast after septation of the filamentous cell vary in size [9, 60], and increase in length in a few hours, generating heterogeneously-sized clonal progeny populations [9] (Fig. S1). As swim-arrest followed by reactivation led to growth delay, thus incurring a fitness cost (Fig. S3), we posit that under uncertain prey supply, these populations may spread the cost by dynamically adjusting the fraction of cells perseverating in swimming, using various swimming strategies.

Remarkably, the observed reactivation responses to single amino acids and to complex mixtures (LB, CAS) (Fig. 2) were similar to those observed when these compounds were tested as attractants in pure cultures [61] or in environmental samples [62], respectively. They also, in all strains, led to rotational/curvilinear dominance, i.e., the swimming patterns found under prey-rich conditions, concomitant with a rapid burst in ATP production (Fig. S4A) in the absence of significant sources of energy. It has been proposed that BALOs use chemotaxis toward nutrients to locate bacteria-rich patches [61] such as flocs and biofilms, with which predators associate [63–65] as chemotaxis toward prey cells in suspension is low [66]. Such behavior may be advantageous in soil and other environments, including on or in plants and animals where prey may find refuge in predator-free patches, and subpopulations of the predator may similarly find themselves confined to patches with no prey or with consumed prey [53]. Moreover, changes in connectivity in the soil are mediated by water and strongly affect *Bdellovibrio* predation [67]. As connectivity rapidly increases with soil wetting but since drying is a much slower process, a rapid response (reactivation) under wetting conditions bringing about the rapid diffusion of prey cues, and slow decay in swimming (swim-arrest) as connectivity breaks down may be advantageous.

Materials and methods

Bacterial strains, media, and growth conditions

Predators: *Bdellovibrio bacteriovorus* HD100 and *Bdellovibrio bacteriovorus* 109J without or with plasmid pMQ414 constitutively expressing the fluorescent tdTomato protein [68], and prey: *E. coli* ML35, *Klebsiella oxytoca*, and *Micrococcus* sp. were grown overnight at 35 and 28 °C, respectively. Growth conditions were essentially as in [28] with slight modifications (Supplementary Materials and Methods).

Synchronous growth

Synchronization of *B. bacteriovorus* cultures was obtained by mixing 10^{10} plaque forming units (PFU) ml^{-1} of the predator with 10^9 CFU ml^{-1} of an exponentially growing *E. coli* ML35 prey in 25 mM Hepes amended with 3 mM $MgCl_2.6H_2O$ and 2 mM $CaCl_2.2H_2O$ (amHEPES) buffer and incubated at 28 °C with shaking at 200 rpm [69]. Under these conditions, prey cells were synchronously attacked and penetrated within 20 min. Synchrony was examined under phase contrast at 1000× magnification at intervals, using an Olympus BX51 microscope (Olympus Corporation, Tokyo, Japan). Fresh attack phase cells (AP1) were released from bdelloplast after 3.5 to 4 h.

Swimming speed trajectory measurement and analysis

Freshly emerged AP cells (AP1) were filtered through a 0.45 µm filter (Millipore, Billerica, MA, USA) to remove residual prey and debris. Their swimming speed and trajectories were measured at constant intervals until swimming halted (arrested AP, aAP2) as in [28]. For details, see Supplementary Materials and Methods.

Swimming behavior in response to starvation

E. coli ML35 or *Klebsiella oxytoca* cells were added to non-swimming aAP2 cells obtained from AP1 cells from synchronous cultures incubated for 8–10 h without prey, to a final concentration of circa 10^6 CFU ml^{-1} and examined by phase contrast microscopy as above. Reactivation of arrested cells (aPA2) at 10^8 PFU ml^{-1} in a final volume of 1 ml was tested by exposing them for various periods of time to LB (1.5%) and CAS amino acids (0.2%) (BD Difco, France) media, and to single amino acids known to attract *B. bacteriovorus* [61]. These included the polar amino acids asparagine, threonine, glutamine, and cysteine and the non-polar amino acids glycine, glutamate, histidine, and lysine (Sigma Aldrich, USA) at final concentrations of 10^{-4}, 10^{-5}, and 10^{-6} M. Swimming speed and trajectories were analyzed, as described in Supplementary Materials and Methods.

Construction of a CRISPR interference (CRISPRi) vector and flagellar-brake gene silencing

For constructing the broad-host range silencing plasmid pRdcas9, pBBR1 ori with a kanamycin resistance gene,

nuclease dead cas9 (dcas9, a endonuclease inactivated version of cas9), single-guide RNA (sgRNA) and the *B. bacteriovorus* HD100 constitutive promoters *bd3749* and *bd0987* were amplified using Q5 High fidelity DNA polymerase (NEB, USA) from pROBE-NT (gift from Steven Lindow; addgene plasmid no. 37818), pJMP1237 (a gift from Oren Rosenberg; addgene plasmid no. 119262) [70], pTargetF (gift from Sheng Yang; addgene plasmid no. 62226) and *B. bacteriovorus* HD100 genomic DNA, respectively. These fragments were assembled using NEBuilder HiFi DNA assembly (NEB, USA) according to the manufacturer's protocol. Constitutive promoters *bd3749* and *bd0987* drive the expression of dCas9 and sgRNA, respectively. SalI, XbaI, and BamH1 were introduced upstream of sgRNA enabling the insertion of 20 bp nucleotide silencing target sequences (Tables S2, S3).

The pRdcas9 was bridged with a 20-nt gene silencing target single-stranded DNA (ssDNA) oligo using NEBuilder® HiFi DNA Assembly (NEB, USA). An 80 base, single-stranded DNA oligonucleotide (IDT, Syntezza, Israel), containing a 20-nt target sequence flanked by a pRdcas9 for *bd0760* or *bd1007* were diluted to 0.2 µM in 1× NEB buffer 2 (Table S3). Five microliter of 0.2 µM ssDNA oligo, 30 ng of the xbaI linearized vector were mixed to a final volume of 10 µl adjusted with ddH_2O. To this, an equal volume of NEBuilder HiFi DNA Assembly master mix was added and the mixture incubated for 1 h at 50 °C. One microliter of the product was electroporated into *E. coli* S17 cells using a MicroPulser electroporator (Bio-Rad, USA) and plated on LB agar supplemented with 50 µg ml^{-1} kanamycin. Integrity of the constructs was screened by colony-PCR and confirmed by sequencing. The plasmids were introduced into *B. bacteriovorus* HD100 by conjugation [40] (Table S2).

Motility assays of overexpressed *bd0760* and *bd1007*

E. coli K12-MG1655 *ycgR*, and *B. bacteriovorus* HD100 *bd1007* and *bd0760* were amplified from genomic DNA by PCR with Q5 high fidelity DNA polymerase (NEB, USA), cloned into an L-arabinose inducible vector pBADgIIIA (Invitrogen, USA), and constructs validated by sequencing (Tables S2, S3). LB swim and swarm plates containing 0.3% and 0.5% Bacto agar, respectively, were supplemented with 100 µg ml^{-1} ampicillin and 0.2% L-arabinose; 0.5% glucose was added to the warm plates [71].

Response time toward prey

B. bacteriovorus HD100 wild type, *ΔmerRNA*, and *ΔdgcC* (a kind gift from Liz Sockett, University of Nottingham), were used in this experiment. µ-Slide Chemotaxis slides (80326, ibidi GmbH, Martinsried, Germany), consisting of two separate liquid chambers, divided by a 1 mm narrow transition zone, were filled with about 10^7 CFU ml^{-1} *E. coli* ML35 in amHEPES in the first reservoir, and about 5×10^9 PFU ml^{-1} non-swimming 10 h long starved aAP2 cells in the second reservoir. Ten times diluted nutrient agar (0.5% agar) was placed in the transition zone. The edge of the *E. coli* chamber adjoining the transition zone was examined under bright field using an inverted microscope (Nikon TiE, Japan) with NIS AR elements software. The time taken for AP cells to migrate from the transition chamber into the *E. coli* chamber was recorded. Three independent experiments were performed.

RNA sequencing and data analysis

RNA was extracted from triplicated biological samples of *B. bacteriovorus* HD100 AP1 and aAP2 cells using a MasterPure™ RNA Purification Kit according to the manufacturer's protocol (Epicenter, USA). RNA concentrations were measured using Quant-iT RiboGreen RNA assay (Life Technologies, Inc.), and RNA quality was assessed using an Agilent 2200 Tapestation with High Sensitivity RNA ScreenTape® (Agilent Technologies, Palo Alto, CA, USA). A 2 µg sample of RNA was depleted of rRNA with the Ribo-Zero rRNA Removal kit for Gram-negative bacteria (Illumina). Library preparation was performed using the TruSeq Stranded Total RNA Library Preparation protocol (Illumina). Libraries were quantified by QPCR using the Illumina Sequencing Library QPCR Quantification protocol guide, version February 2011. Library size distribution and quality were checked on a DNA 1000 chip (Agilent Technologies). Sequencing was performed with a high-throughput Illumina NextSeq 500 flow cell generating 75-bp paired-end reads.

Reads were mapped to the *B. bacteriovorus* HD100 reference genome (NCBI Ref. seq. id. NC_005363.1) with a 95% similarity cutoff by using CLC Genomics Workbench version 10 (Qiagen, Denmark). The differentially expressed genes (DEGs) were calculated according to the standard protocols of CLC Genomics Workbench. Genes were reported as significantly differentially expressed when the FDR P value was <0.05, and there was a change of ≥1.5-fold. Functional analysis of DEGs was performed using Gene Set Enrichment Analysis (GSEA-Pro) web tool (http://server.molgenrug.nl/index.php/gsea-pro). The function of the differentially expressed hypothetical genes was predicted using the SWISS model web server.

For flow cytometry, predation assay, swimming speed trajectory measurement and analysis, ATP quantification, membrane potential measurement, live–dead staining,

*mer*RNA deletion and complementation, and localization of flagellar-brake proteins, see Supplementary Material.

Statistical analysis

Statistical analysis was performed using the JMP Pro (version 15) and GraphPad Prism program (version 8.3). All the data except qPCR were subjected to one-way ANOVA with Tukey's multiple comparison test. The relative transcript levels in qPCR were calculated by normalizing CT values to lon protease (*bd3749*) [72] and plotted as $^{2-}\Delta\Delta$CT. Difference between the AP1 to aAP2 and rAP2 was calculated using Student's *t* test. The swimming trajectory data was subjected to a nonparametric Kolmogorov–Smirnov test to compare the distribution curves. The graphs were plotted using Origin v. 2019b and GraphPad Prism v.8.3.

Acknowledgements This research was supported by the Korea–Israel Cooperative Scientific Research, budget number 3-14168, and by the U.S. Army Research Office and the Defense Advanced Research Projects Agency and was accomplished under Cooperative Agreement Number W911NF-15-2-0036 to DEK, EJ, and AH. The views and conclusions contained in this document are those of the authors and should not be interpreted as representing the official policies, either expressed or implied, of the Army Research Office, DARPA, or the U. S. Government. The U.S. Government is authorized to reproduce and distribute reprints for Government purposes notwithstanding any copyright notation hereon. We would like to thank Menyat Elsayed for her help with the paper.

Compliance with ethical standards

Conflict of interest The authors declare that they have no conflict of interest.

Publisher's note Springer Nature remains neutral with regard to jurisdictional claims in published maps and institutional affiliations.

References

1. Ho A, Di Lonardo DP, Bodelier PLE. Revisiting life strategy concepts in environmental microbial ecology. FEMS Microbiol Ecol. 2017;93:fix006.
2. Poindexter JS. Oligotrophy. In: Alexander M, editor. Advances in microbial ecology. Springer US, Boston, MA: Springer US; 1981. pp. 63–89.
3. Madigan MT, Bender KS, Buckley DH, Sattley WM, Stahl DA. Brock Biology of Microorganisms, 15th Global edition. Boston, US: Benjamin Cummins. 2018.
4. Navarro Llorens JM, Tormo A, Martínez-García E. Stationary phase in gram-negative bacteria. FEMS Microbiol Rev. 2010;34:476–95.
5. Wood TK, Knabel SJ, Kwan BW. Bacterial persister cell formation and dormancy. Appl Environ Microbiol. 2013;79:7116–21.
6. Klotz A, Georg J, Bučinská L, Watanabe S, Reimann V, Januszewski W, et al. Awakening of a dormant cyanobacterium from nitrogen chlorosis reveals a genetically determined program. Curr Biol. 2016;26:2862–72.
7. Setlow P, Wang S, Li Y-Q. Germination of spores of the orders *Bacillales* and *Clostridiales*. Annu Rev Microbiol. 2017;71:459–77.
8. Song S, Wood TK. ppGpp ribosome dimerization model for bacterial persister formation and resuscitation. bioRxiv. 2019. https://doi.org/10.1101/663658.
9. Fenton AK, Kanna M, Woods R, Aizawa S, Sockett RE. Shadowing the actions of a predator: Backlit fluorescent microscopy reveals synchronous nonbinary septation of predatory *Bdellovibrio* inside prey and exit through discrete bdelloplast pores. J Bacteriol. 2010;192:6329–35.
10. Makowski Ł, Donczew R, Weigel C, Zawilak-Pawlik A, Zakrzewska-Czerwinska J. Initiation of chromosomal replication in predatory bacterium *Bdellovibrio bacteriovorus*. Front Microbiol. 2016;7.
11. Rotem O, Pasternak Z, Jurkevitch E. The genus *Bdellovibrio* and like organisms. The prokaryotes: deltaproteobacteria and epsilonproteobacteria. 2014. pp. 3–17.
12. Lambert C, Evans KJ, Till R, Hobley L, Capeness M, Rendulic S, et al. Characterizing the flagellar filament and the role of motility in bacterial prey-penetration by *Bdellovibrio bacteriovorus*. Mol Microbiol. 2006;60:274–86.
13. Thomashow LS, Rittenberg SC. Waveform analysis and structure of flagella and basal complexes from *Bdellovibrio bacteriovorus* 109J. J Bacteriol. 1985;163:1038–46.
14. Hespell RB, Rosson RA, Thomashow MF, Rittenberg SC. Respiration of *Bdellovibrio bacteriovorus* strain 109J and its energy substrates for intraperiplasmic growth. J Bacteriol. 1973;113:1280–8.
15. Hespell RB, Thomashow MF, Rittenberg SC. Changes in cell composition and viability of *Bdellovibrio bacteriovorus* during starvation. Arch Microbiol. 1974;97:313–27.
16. Paix B, Ezzedine JA, Jacquet S. Diversity, dynamics, and distribution of *Bdellovibrio* and like organisms in perialpine lakes. Appl Environ Microbiol. 2019;85.
17. Varon M, Fine M, Stein A. The maintenance of *Bdellovibrio* at low prey density. Microb Ecol. 1984;10:95–8.
18. Varon M, Zeigler BP. Bacterial predator-prey interaction at low prey density. Appl Environ Microbiol. 1978;36:11–7.
19. Chen H, Young S, Berhane TK, Williams HN. Predatory *Bacteriovorax* communities ordered by various prey species. PLoS ONE. 2012;7.
20. Rogosky AM, Moak PL, Emmert EAB. Differential predation by *Bdellovibrio bacteriovorus* 109J. Curr Microbiol. 2006;52:81–5.
21. Jurkevitch E, Minz D, Ramati B, Barel G. Prey range characterization, ribotyping, and diversity of soil and rhizosphere *Bdellovibrio* spp. isolated on phytopathogenic bacteria. Appl Environ Microbiol. 2000;66:2365–71.
22. Kandel PP, Pasternak Z, van Rijn J, Nahum O, Jurkevitch E. Abundance, diversity and seasonal dynamics of predatory bacteria in aquaculture zero discharge systems. FEMS Microbiol Ecol. 2014;89:149–61.
23. Pineiro SA, Williams HN, Stine OC, Piñeiro SA, Williams HN, Stine OC. Phylogenetic relationships amongst the saltwater members of the genus *Bacteriovorax* using rpoB sequences and reclassification of *Bacteriovorax stolpii* as *Bacteriolyticum stolpii* gen. nov., comb. nov. Int J Syst Evol Microbiol. 2008;58:1203–9.
24. Chen H, Athar R, Zheng G, Williams HN. Prey bacteria shape the community structure of their predators. ISME J. 2011;5:1314–22.
25. Shatzkes K, Connell ND, Kadouri DE. Predatory bacteria: a new therapeutic approach for a post-antibiotic era. Future Microbiol. 2017;12:469–72.
26. Guo Y, Yan L, Cai J. Effects of *Bdellovibrio* and like organisms on survival and growth performance of juvenile turbot, scophthalmus maximus. J World Aquac Soc. 2016;47:633–45.

27. Youdkes D, Helman Y, Burdman S, Matan O, Jurkevitch E. Potential control of potato soft rot disease by the obligate predators *Bdellovibrio* and like organisms. Appl Environ Microbiol. 2020;86.
28. Sathyamoorthy R, Maoz A, Pasternak Z, Im H, Huppert A, Kadouri D, et al. Bacterial predation under changing viscosities. Environ Microbiol. 2019;21:2997–3010.
29. Hobley L, Fung RKY, Lambert C, Harris MATS, Dabhi JM, King SS, et al. Discrete cyclic di-GMP-dependent control of bacterial predation versus axenic growth in *Bdellovibrio bacteriovorus*. PLoS Pathog. 2012;8.
30. Karunker I, Rotem O, Dori-Bachash M, Jurkevitch E, Sorek R. A global transcriptional switch between the attack and growth forms of *Bdellovibrio bacteriovorus*. PLoS ONE. 2013;8.
31. Amikam D, Galperin MY. PilZ domain is part of the bacterial c-di-GMP binding protein. Bioinformatics. 2006;22:3–6.
32. Ko J, Ryu K-S, Kim H, Shin J-S, Lee J-O, Cheong C, et al. Structure of PP4397 reveals the molecular basis for different c-di-GMP binding modes by PilZ domain proteins. J Mol Biol. 2010;398:97–110.
33. Wirebrand L, Österberg S, López-Sánchez A, Govantes F, Shingler V. PP4397/FlgZ provides the link between PP2258 c-di-GMP signalling and altered motility in *Pseudomonas putida*. Sci Rep. 2018;8:1–10.
34. Shanks RMQ, Davra VR, Romanowski EG, Brothers KM, Stella NA, Godboley D, et al. An eye to a kill: using predatory bacteria to control gram-negative pathogens associated with ocular infections. PLOS ONE. 2013;8:e66723.
35. Wurtzel O, Dori-Bachash M, Pietrokovski S, Jurkevitch E, Sorek R. Mutation detection with next-generation resequencing through a mediator genome. PLoS ONE. 2010;5.
36. Pasternak Z, Njagi M, Shani Y, Chanyi R, Rotem O, Lurie-Weinberger MN, et al. In and out: an analysis of epibiotic vs periplasmic bacterial predators. ISME J. 2014;8:625–35.
37. Pletnev P, Osterman I, Sergiev P, Bogdanov A, Dontsova O. Survival guide: *Escherichia coli* in the stationary phase. Acta Nat. 2015;7:22–33.
38. Kazmierczak MJ, Wiedmann M, Boor KJ. Alternative sigma factors and their roles in bacterial virulence. Microbiol Mol Biol Rev. 2005;69:527–43.
39. Paget MS. Bacterial sigma factors and anti-sigma factors: structure, function and distribution. Biomolecules. 2015;5:1245–65.
40. Avidan O, Petrenko M, Becker R, Beck S, Linscheid M, Pietrokovski S, et al. Identification and characterization of differentially-regulated type IVb pilin genes necessary for predation in obligate bacterial predators. Sci Rep. 2017;7:1–12.
41. Barembruch C, Hengge R. Cellular levels and activity of the flagellar sigma factor FliA of Escherichia coli are controlled by FlgM-modulated proteolysis. Mol Microbiol. 2007;65:76–89.
42. Rendulic S, Jagtap P, Rosinus A, Eppinger M, Baar C, Lanz C, et al. A predator unmasked: life cycle of *Bdellovibrio bacteriovorus* from a genomic perspective. Science. 2004;303:689–92.
43. Nyström T. Stationary-phase physiology. Annu Rev Microbiol. 2004;58:161–81.
44. Browning AP, Sharp JA, Mapder T, Baker CM, Burrage K, Simpson MJ. Persistence is an optimal hedging strategy for bacteria in volatile environments. bioRxiv. 2019. https://doi.org/10.1101/2019.12.19.883645.
45. Ratcliff WC, Denison RF. Individual-level bet hedging in the bacterium *Sinorhizobium meliloti*. Curr Biol. 2010;20:1740–4.
46. Zhang X-X, Rainey PB. Bet hedging in the underworld. Genome Biol. 2010;11:137.
47. Franklin RB, Mills AL. Multi-scale variation in spatial heterogeneity for microbial community structure in an eastern Virginia agricultural field. FEMS Microbiol Ecol. 2003;44:335–46.
48. Manderscheid B, Matzner E. Spatial heterogeneity of soil solution chemistry in a mature Norway spruce (Picea abies (L.) Karst.) stand. Water Air Soil Pollut. 1995;85:1185–90.
49. Ranjard L, Lejon DPH, Mougel C, Schehrer L, Merdinoglu D, Chaussod R. Sampling strategy in molecular microbial ecology: Influence of soil sample size on DNA fingerprinting analysis of fungal and bacterial communities. Environ Microbiol. 2003;5:1111–20.
50. Jenal U, Reinders A, Lori C. Cyclic di-GMP: second messenger extraordinaire. Nat Rev Microbiol. 2017;15:271–84.
51. Boehm A, Kaiser M, Li H, Spangler C, Kasper CA, Ackermann M, et al. Second messenger-mediated adjustment of bacterial swimming velocity. Cell. 2010;141:107–16.
52. Paul K, Nieto V, Carlquist WC, Blair DF, Harshey RM. The c-di-GMP binding protein YcgR controls flagellar motor direction and speed to affect chemotaxis by a 'Backstop Brake' mechanism. Mol Cell. 2010;38:128–39.
53. Dattner I, Miller E, Petrenko M, Kadouri DE, Jurkevitch E, Huppert A. Modelling and parameter inference of predator–prey dynamics in heterogeneous environments using the direct integral approach. J R Soc Interface. 2017;14:20160525.
54. Hol FJH, Rotem O, Jurkevitch E, Dekker C, Koster DA. Bacterial predator–prey dynamics in microscale patchy landscapes. Proc R Soc B Biol Sci. 2016;283:20152154.
55. Gabel CV, Berg HC. The speed of the flagellar rotary motor of *Escherichia coli* varies linearly with protonmotive force. Proc Natl Acad Sci USA. 2003;100:8748–51.
56. Gadkari D, Stolp H. Energy metabolism of *Bdellovibrio bacteriovorus*. I. Energy production, ATP pool, energy charge. Arch Microbiol. 1975;102:179–85.
57. Shioi JI, Galloway RJ, Niwano M, Chinnock RE, Taylor BL. Requirement of ATP in bacterial chemotaxis. J Biol Chem. 1982;257:7969–75.
58. Fang X, Gomelsky M. A post-translational, c-di-GMP-dependent mechanism regulating flagellar motility. Mol Microbiol. 2010;76:1295–305.
59. Varon M. Interaction of *Bdellovibrio* with its prey in mixed microbial populations. Microb Ecol. 1981;7:97–105.
60. Kessel M, Shilo M. Relationship of *Bdellovibrio* elongation and fission to host cell size. J Bacteriol. 1976;128:477–80.
61. LaMarre AG, Straley SC, Conti SF. Chemotaxis toward amino acids by *Bdellovibrio bacteriovorus*. J Bacteriol. 1977;131:201–7.
62. Chauhan A, Williams HN. Response of *Bdellovibrio* and like organisms (BALOs) to the migration of naturally occurring bacteria to chemoattractants. Curr Microbiol. 2006;53:516–22.
63. Feng S, Tan CH, Constancias F, Kohli GS, Cohen Y, Rice SA. Predation by *Bdellovibrio bacteriovorus* significantly reduces viability and alters the microbial community composition of activated sludge flocs and granules. FEMS Microbiol Ecol. 2017;93.
64. Kadouri DE, O'Toole GA. Susceptibility of biofilms to *Bdellovibrio bacteriovorus* attack. Appl Environ Microbiol. 2005;71:4044–51.
65. Szabó E, Liébana R, Hermansson M, Modin O, Persson F, Wilén B-MB-MB-M, et al. Comparison of the bacterial community composition in the granular and the suspended phase of sequencing batch reactors. AMB Express. 2017;7:168.
66. Lambert C, Smith MCM, Sockett RE. *A novel assay to monitor predator-prey interactions for Bdellovibrio bacteriovorus* 109 J reveals a role for methyl-accepting chemotaxis proteins in predation. Environ Microbiol. 2003;5:127–32.
67. Petrenko M, Friedman SP, Fluss R, Pasternak Z, Huppert A, Jurkevitch E. Spatial heterogeneity stabilizes predator–prey interactions at the microscale while patch connectivity controls their outcome. Environ Microbiol. 2019;22:694–704.

68. Mukherjee S, Brothers KM, Shanks RMQQ, Kadouri DE. Visualizing *Bdellovibrio bacteriovorus* by using the tdTomato fluorescent protein. Appl Environ Microbiol. 2015;82:1653–61.
69. Jurkevitch E. Isolation and classification of *Bdellovibrio* and like organisms. Curr Protoc Microbiol. 2012;Chapter 7:Unit 7B.1.
70. Peters JM, Koo B-M, Patino R, Heussler GE, Hearne CC, Qu J, et al. Enabling genetic analysis of diverse bacteria with Mobile-CRISPRi. Nat Microbiol. 2019;4:244–50.
71. Copeland MF, Weibel DB. Bacterial swarming: a model system for studying dynamic self-assembly. Soft Matter. 2009;5: 1174–87.
72. Rotem O, Pasternak Z, Shimoni E, Belausov E, Porat Z, Pietrokovski S, et al. Cell-cycle progress in obligate predatory bacteria is dependent upon sequential sensing of prey recognition and prey quality cues. Proc Natl Acad Sci. 2015;112: E6028–37.